DOI: 10.1021/cg1000864

CRYSTAL GROWTH & DESIGN Article

2010, Vol. 10
3022–3035

Interactions between Organophosphonate-Bearing Solutions and (10$\bar{1}$4) Calcite Surfaces: An Atomic Force Microscopy and First-Principles Molecular Dynamics Study

Encarnación Ruiz-Agudo,*,† Devis Di Tommaso,‡ Christine V. Putnis,† Nora H. de Leeuw,‡ and Andrew Putnis†

†*Institut für Mineralogie, Universitat Münster, Corrensstrasse 24, 48149, Münster, Germany, and* ‡*Department of Chemistry, University College London, 20 Gordon Street, London, WC1H 0AJ, United Kingdom*

Received January 20, 2010; Revised Manuscript Received April 19, 2010

ABSTRACT: The dissolution of (10$\bar{1}$4) calcite surfaces was investigated in the presence of 1-hydroxy ethylidene-1,1-diphosphonic acid) (HEDP) (0−10 mM) at pH = 8 using in situ atomic force microscopy (AFM). The presence of the organophosphonate resulted in a change in the appearance of the dissolution features from the typical rhombohedral to elongated, tear shapes. Additionally, dissolution rates were drastically reduced, although they progressively increased with increasing additive concentration. Stabilization of polar steps and effects of HEDP on the structure and dynamics of the hydration shell of Ca^{2+} may explain such observations. First principles molecular dynamics simulations have been used to study such aspects. The results suggest that the presence of HEDP can increase the frequency of water exchange in the hydration shell of calcium and consequently affect its reactivity in solution. For [HEDP] > 5 mM, we observed the nucleation and growth of $Ca(CH_3C(OH)(PO_3H)_2 \cdot 2H_2O$ on calcite surfaces. The reaction between solid calcite and HEDP solutions seems to be controlled by the composition of a boundary layer at the carbonate−fluid interface. Dissolution of the carbonate causes this fluid boundary layer to become supersaturated with respect to the phosphonate phase, which then precipitates. The presence of this overgrowth reduces the calcite dissolution rate, thus representing a new treatment aimed at reducing solution-induced weathering of building stone via the formation of a protective nanofilm.

Introduction

In nature, organic molecules often control the nucleation and growth of inorganic phases. Among these minerals calcite and aragonite have the most widespread occurrence, which has motivated numerous studies on the interaction between organic molecules and calcite. While many works have explored the effect of organics on the precipitation of calcite, considerably fewer studies have dealt with the influence of organic molecules on the dissolution of calcite (see the review by Morse et al.[1]). During calcite dissolution and growth in the presence of organics, processes such as adsorption at the carbonate surface or coprecipitation of the organic material with calcium carbonate are generally considered to explain the observed mineral behavior. However, changes in the solvent structure or ion hydration induced by the presence of organic molecules in solution and how they affect crystal dissolution and growth have received little attention. In this sense, the system phosphonate−calcite interaction may be used as a general model for the study of the mechanism of organic−inorganic interactions.

Many current problems in geology or engineering would benefit from gaining a more detailed and fundamental understanding of the interaction between phosphonates and calcite. Phosphonates have been used as scale and corrosion control additives, as well as dispersants, cleaning agents, chelating agents, and crystal growth modifiers.[2] They are stronger complexing agents than carboxylic acids, with the complexation constants increasing with the number of phosphonate groups per molecule. Di- and trivalent cations such as Ca^{2+}, Fe^{3+}, and Al^{3+} are precipitated by phosphonates, especially at circumneutral pH values.[3] The surface chemistry of phosphonates is also important as they are known to adsorb onto silica and clays, barite, cassiterite, aluminum oxides, iron oxides, and calcite.[2,4] The application of phosphonates has made it possible to control the crystallization of sparingly soluble phases which pose significant problems in the oil industry and in water treatment. In this respect, calcite is one of the major scaling minerals affecting the production of petroleum, and adsorption/precipitation of Ca-phosphonate phases in carbonate reservoirs has been proposed as a way of slowly releasing the compound for the inhibition of calcite scale formation from the porous media.[5] Phosphonates also appear naturally in plants, animals, and soils, but increasing amounts of synthetic phosphonates are entering the environment owing to their use as chelating agents and herbicides.[3] Phosphonates released in the environment may interact with minerals in the soil or in porous oil reservoirs.

Apart from geological and engineering applications, diphosphonates are commonly used as therapeutic agents because they effectively inhibit the resorption of the bone, which commonly occurs in diseases such as osteoporosis, Paget's disease, and osteosarcoma.[6] Moreover, clinical research has shown that diphosphonates possess the ability to reduce skeletal-related complications associated with metastatic breast cancer.[7] It has been suggested that these therapeutic properties are due to the ability of diphosphonate molecules to inhibit the precipitation of calcium salts,[8] which is important because bone metastasis often leads to raised serum calcium levels.[9]

*To whom correspondence should be addressed. E-mail: eruiz_01@uni-muenster.de. Tel: +49 (0)251 83 36107. Fax: +49 (0)251 83 38397.

 Published on Web 06/04/2010

Another proposed application of organophosphonates is their use to halt and/or mitigate salt weathering affecting our cultural heritage.[10,11] This is a substantial hazard for historical and cultural built structures and statuary, as well as to modern buildings and engineering constructions, because such salt weathering contributes to the deterioration of concrete and building stone. Calcite is the major component of marbles and limestone, in widespread use as building and ornamental materials. Although physical processes (i.e., crystallization pressure) have been traditionally considered as the main factors responsible for stone damage associated with salts, chemical dissolution is also a major factor contributing to rock weathering. Molecules and ions present in solutions in contact with rocks can affect dissolution of minerals. Recently, it has been suggested that phosphonates may help to reduce damage to stone due to dissolution induced by salts through the formation of a passivating layer.[12] However, no insights into the composition or the formation mechanisms of such layers are as yet available.

The purpose of this paper is therefore to study the nanoscale processes occurring during the interaction of calcite cleavage surfaces and phosphonate-bearing solutions. Several experimental[3,13,14] and computational[15,16] studies have attempted to describe the effects of phosphonates on calcite nucleation and growth. As suggested by Teng and Dove,[17] dissolution features may represent an indication of the crystal faces that become stabilized during mineral growth. However, to our knowledge there are few dissolution studies aimed at testing the mechanism by which 1-hydroxy ethylidene-1,1-diphosphonic acid (HEDP) modifies the reactivity of calcite surfaces.[18,19] The study by Britt and Hlady[18] deals mainly with changes in etch pit morphology induced by the presence of HEDP, and its effect on the kinetics of calcite dissolution is not quantified. In a later work, Kanellopoulou and Koutsoukos[19] measured dissolution rates of a natural polycrystalline calcitic material (marble) in the presence of HEDP, showing a reduction in the kinetics of the process. These studies considered that phosphonate molecules modify calcite dissolution and growth by incorporation at steps, formation of surface complexes, or even precipitation of Ca-HEDP phases, frequently neglecting the effects of these molecules on calcium hydration on the mineral surface or in solution.

We used in situ atomic force microscopy (AFM) as the optimal technique to give insights into the mechanism of such interaction, as well as allowing quantitative measurements of the kinetics of the process. Moreover, we have performed first principles molecular dynamics simulations of Ca^{2+} in water and of Ca^{2+}/$HEDP^{3-}$ aqueous solutions in order to investigate the effect of HEDP molecules on the structural and dynamic properties of the calcium hydration sphere. The knowledge gained through this study will have a direct application in a wide range of fields where the presence of organic molecules may affect the growth and/or dissolution of mineral species, including biomineralization, medicine, the oil and cement industry, and cultural heritage conservation.

Materials and Methods

(a). In Situ AFM Experiments. Direct observation and measurements of calcite single crystal dissolution were made using a Digital Instruments Nanoscope III AFM working in contact mode. Scanning frequency was 3.81 Hz, and scanning areas were 5×5 and 10×10 μm. AFM images were usually taken by scanning conical Si_3N_4 tips. Optically clear Iceland Spar calcite (Mexico) crystals, with $(10\bar{1}4)$ directly cleaved before each experiment to produce samples approximately $4 \times 4 \times 0.6$ mm in size, were used as substrates. Before each dissolution experiment, deionized water was passed over the crystal to clean the cleaved surface, as well as to adjust the AFM parameters. Solutions were prepared from HEDP 60% solutions (Sigma-Aldrich) diluted in distilled deionized (18 mΩ) water down to concentrations ranging from 0.01 up to 10 mM. The pH was adjusted to 8 using granulated NaOH. In a first set of experiments, solutions were flowed continuously at 60 mL h^{-1} from a syringe through an O-ring-sealed fluid cell containing the sample crystal. Shiraki et al.[20] have shown that for pH > 5.3 the velocity of step retreat is independent of flow rate for values higher than 29 mL h^{-1} (at room temperature and $pCO_2 \approx 10^{-3.5}$ atm), and thus dissolution was limited not by diffusive transport but by surface processes in our experiments. In a second set of experiments, 0.75 mM HEDP solutions were flowed continuously at 6, 30, 60, and 90 mL h^{-1}. Finally, 10 mM HEDP solutions were put in contact with calcite surfaces with no flow through the system (i.e., using the AFM as a batch reactor). Dissolution rates were inferred from step retreat velocities (or etch pit spreading rates). Such measurements were made using the NanoScope software (version 5.12b48). Step velocity measurements were always made from images scanned in the same direction. The retreat velocity was calculated by measuring the length increase per unit time along a fixed direction in sequential images. Additionally, after flowing through the fluid cell 10 mL aliquots of effluent solution were collected for calcium analysis by inductively coupled plasma optical emission spectrometry, ICP-OES (Varian Vista pro-axial). Macroscopic dissolution rates of calcite, R_{mac} (mol cm^{-2} s^{-1}) were calculated as follows:

$$R_{mac} = \frac{Ca_T Q}{A} \quad (1)$$

where Ca_T is the total calcium in the effluent solution (mol L^{-1}), Q is the solution flow rate (L s^{-1}), and A is the geometric area of calcite exposed to the solution (cm^2). In flow through experiments performed in AFM, variations and uncertainties related to the reacting surface area contribute to significant error in macroscopic rate determinations,[21] typically leading to an overestimation of macroscopic dissolution rates.[22] Thus, here we present a few selected R_{mac} values only for comparison purposes.

(b). Analysis of Precipitates. Iceland spar crystals after contact with HEDP aqueous solutions of concentrations ranging from 0 up to 10 mM (pH = 8) were analyzed using a Philips PW-1547 X-ray diffractometer with an automatic slit, Cu Kα radiation (λ = 1.5405 Å), 3 to 60° 2θ explored area, with steps of 0.005° 2θ and 4 s counting time (static mode). Following contact with HEDP-bearing solutions, crystals were gently rinsed with deionized water, dried at room temperature, and placed in the diffractometer chamber with their $(10\bar{1}4)$ cleavage plane parallel to the sample holder. XRD analyses were aimed at detecting the formation of HEDP phases and any possible epitaxial relationship between product and parent phases.

(c). First-Principles Molecular Dynamics Simulations. Car–Parrinello molecular dynamics simulations[23] of Ca^{2+} and not-associated Ca^{2+}/$HEDP^{3-}$ in water were carried out using the CP code included in the Quantum-ESPRESSO package, version 4.0.1.[24] Perdew–Burke–Ernzerhof (PBE) gradient corrected functional[25] was applied along with the Vanderbilt ultrasoft pseudopotentials (USPP).[26] The electronic wave functions were expanded in a plane wave (PW) basis set with a kinetic energy cutoff of 30 Ry. The USPP for C and Ca was taken from the standard Quantum-ESPRESSO distribution, whereas the USPP for O, H, and P were generated using the USPP 7.3 pseudopotential program with a scalar-relativistic calculation.[27] The time step for simulations was set to 0.12 fs and the electronic mass was set to 600 au. All simulations were carried out in the NVT ensemble using a Nosé–Hoover chain thermostat[28] to maintain the average temperature at T = 400 K, which is necessary to obtain a liquid-like water structure and diffusion time scales when using gradient corrected density functionals.[29] The isotopic mass of deuterium was used for hydrogen.

CP-MD simulations of aqueous solutions of Ca^{2+} were conducted on a single ion embedded in a box with 83 water molecules, which was generated by taking the last configuration of 6 ps of CP-MD simulation of 84 heavy water molecules in a cubic supercell with a side length of 13.84 Å, which corresponds to the extrapolated

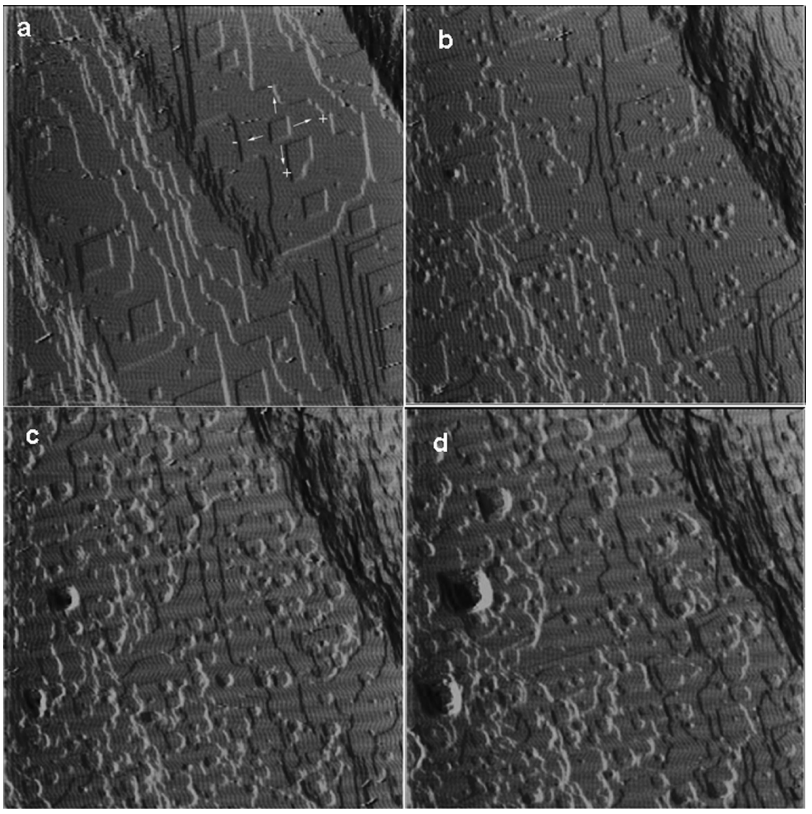

Figure 1. Sequence of AFM deflection images of a calcite ($10\bar{1}4$) surface in (a) water, (b−d) 0.5 mM HEDP pH 8. All images are $5 \times 5\,\mu$m. Note the change in etch pit morphology from rhombohedral to tear-shaped when HEDP is present.

experimental density of heavy water at 400 K,[29] and replacing one Ca^{2+} ion with one H_2O molecule. The aqueous solutions of Ca^{2+}/$HEDP^{3-}$ were generated from a previous CP-MD simulation of $HEDP^{3-}$ in 78 H_2O by substituting one H_2O with one Ca^{2+} at two different positions: $d_{(Ca-C^*)}$ = 6.6 Å (simulation A) and 8.9 Å (simulation B), where C* is the central carbon atom of the $HEDP^{3-}$ molecule, as both correspond to initial configurations where $HEDP^{3-}$ is outside the coordination shell of the calcium ion. These two configurations were selected in order to simulate the effect of HEDP concentration. Shorter Ca−C* distances represent higher HEDP concentrations. For all simulations, the statistics were collected for ~20 ps.

The exchange processes of the water molecules in the first and second hydration shell of the calcium ion during the CP-MD simulations of the aqueous solutions of Ca^{2+} and Ca^{2+}/$HEDP^{3-}$ have been quantified using the "direct" method.[29] In this method, the trajectory of the molecular dynamics simulation is scanned for movements of water molecules, either entering or leaving a coordination shell. Whenever a ligand crosses the boundaries of this shell, its path is followed and if its new position outside/inside the shell lasts for more than a time parameter t^*, the event is accounted as real. For the time parameter t^*, we have chosen the value of 0.5 ps because this has been shown to give a good measure of ligand exchange processes.[30]

Results

(a). Atomic Force Microscopy Observations of Surface Topography. Once pure water was flowed through the fluid cell, initiation of the dissolution process was evident from the immediate formation of discrete pits in the calcite surface. A representative image of an etch pit on the calcite ($10\bar{1}4$) surface following dissolution by pure water is shown in Figure 1a. Etch pits are rhombohedral (diagonal length ratio, [$42\bar{1}$]/[010] ~ 0.7), flanked by steps aligned along the [$48\bar{1}$] and [$\bar{4}41$] directions, that form obtuse and acute angles with the bottom

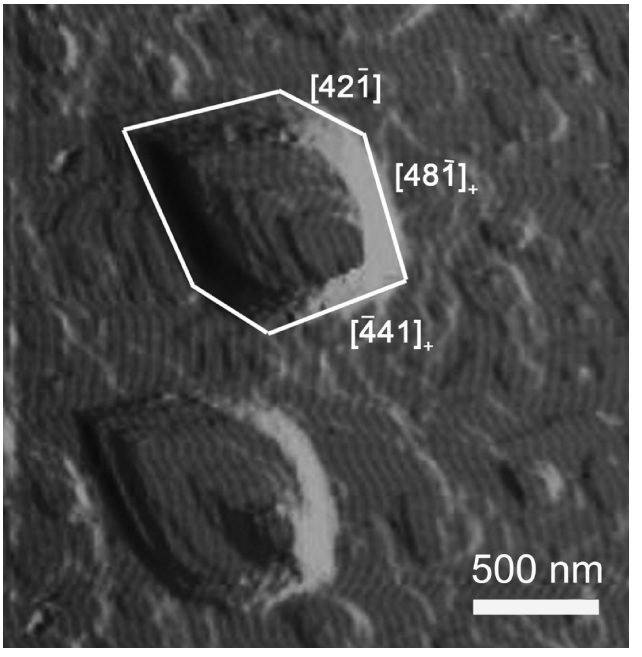

Figure 2. Detail of etch pit morphology in the presence of 0.5 mM HEDP, pH 8.

of the step (102° and 78°). The morphology of the pit formed is similar to that frequently described for calcite cleavage surfaces in previous studies (see for example the work by Astilleros et al.[31]). Steps are mainly one monolayer (~3 Å high). The same area of the crystal was then observed after the water was replaced by HEDP solutions. This produced a rapid

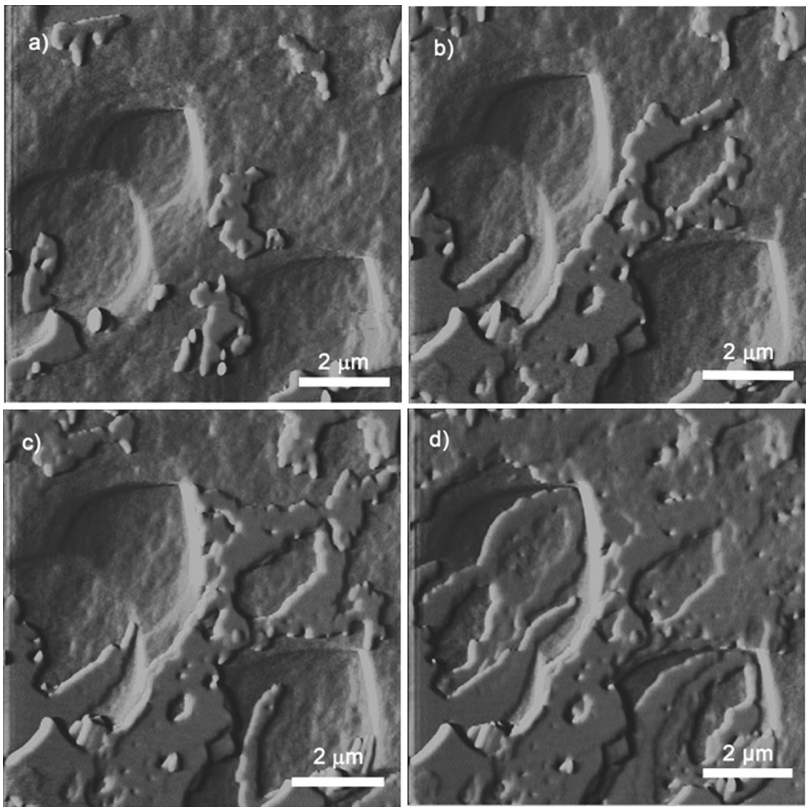

Figure 3. Sequence of AFM deflection images showing three-dimensional island nucleation and growth on a calcite cleavage surface in contact with a 10 mM HEDP solution (pH 8). The initial nucleated islands coalesce forming a layer that almost covers the whole surface reproducing its initial surface topography. Simultaneously, dissolution of calcite occurs as can be deduced from the observed widening of the etch pits.

nucleation of new etch pits. Increasing HEDP concentration leads to a general increase in etch pit density. Figure 1 shows a time sequential image set (deflection signal) of a $5 \times 5\ \mu$m area where initially etch pits with straight sides formed in the presence of water (Figure 1a). Afterward, the same area was exposed to 0.5 mM HEDP solution, leading to the formation of elongated, tear-shaped etch pits (Figure 1b−d). As shown in detail in Figure 2, this change in morphology upon addition of HEDP is the result of the development of new step edges parallel to $[42\bar{1}]$. Additionally, the two obtuse (+) steps become curved and lose their well-defined directions, while the two acute (−) steps remain unaffected, as a result of pinning of the +/+ corner. This morphology is in agreement with that described by Britt and Hlady[18] in the presence of 10 μM HEDP. They observed rhombohedral etch pits with slightly curved +/− and +/+ corners.

For concentrations above 5 mM, dissolution of calcite in the presence of HEDP was accompanied by nucleation of a new phase on the calcite surface. These nuclei or three-dimensional islands reached a thickness of 4.1 ± 0.3 nm during the very early stages of their formation. They rarely showed well-defined straight edges and occasionally pseudohexagonal morphologies were detected (Figure 3a). In batch experiments, once the initial nucleation event occurred, no further nucleation was observed. The growth of this new phase occurred by lateral spreading of the 3D islands, without a significant increase of their height that remained approximately constant during the whole growth process. Eventually, the growth of the nuclei leads to their coalescence (Figure 3d). A nanometric layer, that almost completely covered the observed calcite surface, formed. Initially, the growth of this layer avoided the areas where etch pits previously existed, leading to the formation of a surface almost identical to the original calcite surface. Although AFM experiments do not report compositional information of the precipitating phase, ex-situ XRD analysis of the overgrowth allowed identification of the newly formed phase as $Ca(CH_3C(OH)(PO_3H)_2)\cdot 2H_2O$. Two distinct Ca-HEDP precipitates are described in the literature, having 1:1 (CaHEDP) and 2:1 (Ca_2HEDP) calcium/HEDP molar ratios. The first one is crystalline and its molecular formula is $Ca(CH_3C(OH)(PO_3H)_2)\cdot 2H_2O$, while the second one is amorphous.[32] XRD analysis of the calcite surface after long-term contact (i.e., one week) with a 5 mM HEDP solution (ex-situ experiments) showed that the new phase formed on the calcite cleavage plane was crystalline. The XRD pattern of the overgrowth is shown in Figure 4. Diffraction data of the crystalline 1:1 Ca-phosphonate phase was found in Browning and Fogler.[32] The XRD pattern of $Ca(CH_3C(OH)(PO_3H)_2)\cdot 2H_2O$ was indexed with the help of the Crystal Diffraction software, included in the Crystal Maker program (www.crystalmaker.com) using the crystal structure data proposed by Uchtmann.[33] The slight increase in the relative intensity of the 001 reflection indicates some preferential orientation of the Ca-phosphonate phase, with its (001) plane parallel to the calcite cleavage plane.

(b). Effect of HEDP on Etch Pit Spreading Rates. Because of the irregular shape of the pits, comparisons of spreading rates measured in pure water with those carried out in solutions containing HEDP could not be accomplished by measuring the advancement of the typical $[\bar{4}41]$ and $[48\bar{1}]$ rhombohedral edges. Therefore, it was decided to quantify the expansion rate of the etch pits from the change in length of the two main diagonals ($[42\bar{1}]$ and [010]) of the rhombus. It

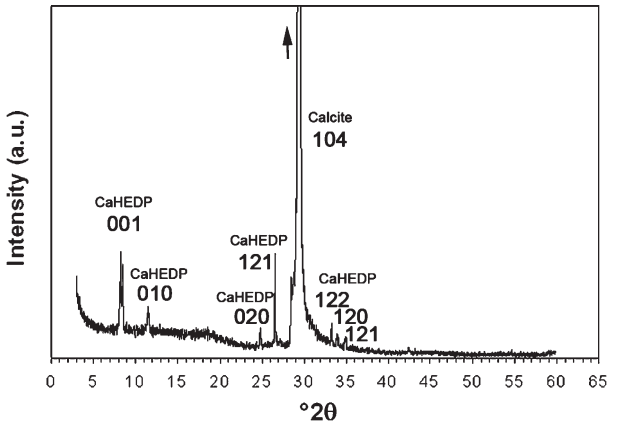

Figure 4. XRD pattern of calcite crystal oriented with the $(10\bar{1}4)$ cleavage plane parallel to the sample holder after 1 week contact with 5 mM HEDP solutions (pH 8) in batch reactors.

Table 1. Spreading Rates (v, nm s^{-1}) along the [42$\bar{1}$] and [010] Diagonals of Etch Pits Nucleated on Calcite {10$\bar{1}$4} Terraces vs. HEDP Concentration

	[42$\bar{1}$]		[010]	
[HEDP] (mM)	v	std	v	std
0.00	2.74	0.17	3.26	0.06
0.01	0.30	0.23	0.40	0.06
0.10	0.71	0.11	0.59	0.17
0.25	0.65	0.25	0.35	0.15
0.75	0.74	0.26	0.70	0.16
1.00	0.84	0.12	0.78	0.13
5.00	1.54	0.26	1.05	0.20
10	2.88	0.24	2.18	0.18

was found that the presence of HEDP (0.01 mM) resulted in a drastic reduction in the expansion rate along both the [42$\bar{1}$] and [010] diagonals compared to pure water, from 2.74 ± 0.17 and 3.26 ± 0.06 nm s^{-1} to 0.30 ± 0.23 and 0.40 ± 0.06 nm s^{-1}, respectively (Table 1 and Figure 5). The change in the ratio of the [42$\bar{1}$] to [010] spreading rates to values above 1 in the presence of HEDP reflects the tendency of etch pits to elongate along the [42$\bar{1}$] direction. However, upon increasing the phosphonate concentration, a continuous rise in etch pit spreading rates was observed. Figure 6 shows the etch pit spreading rate measured at different flow rates of the solution over the calcite surface in the fluid cell (for a constant additive concentration of 0.75 mM). Increasing the flow rate from 6 to 60 mL h^{-1} results in a continuous decrease in the calcite dissolution rate. For values above 60 mL h^{-1}, the rate was found to be independent of the solution flow rate.

(c). Dissolution Rates from Calcium Fluxes. Table 2 and Figure 7 show values of R_{mac} and log R_{mac} calculated from ICP-OES measurements of Ca_T concentration in effluent solution using eq 1. The calculated log R_{mac} for deionized water was −9.61(±0.10). This value is in agreement with those found in the literature for calcite dissolution under similar conditions (see for example the paper by Shiraki and co-workers,[20] who reported a log R_{mac} value of −9.5 for Iceland spar dissolution in water at circumneutral pH and at room temperature and low pCO_2). Values of R_{mac} increased with HEDP concentration in the inlet solution from 2.78×10^{-11} ($\pm 2.94 \times 10^{-12}$) to 8.03×10^{-10} ($\pm 8.82 \times 10^{-12}$) mol cm^{-2} s^{-1}. Note that the rate of calcite dissolution in 0.01 and 0.1 mM HEDP solution (pH = 8) is considerably lower than that found for deionized water. This trend is in agreement

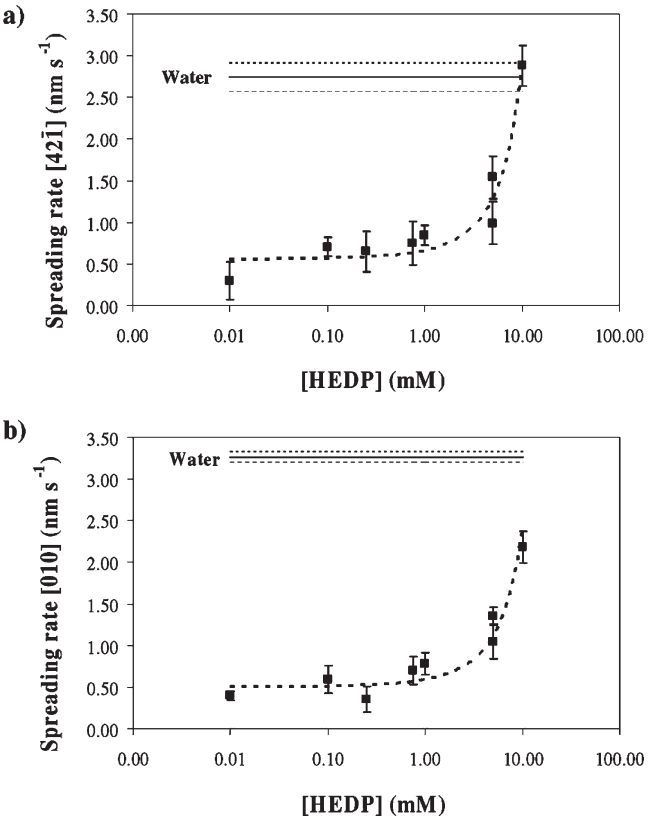

Figure 5. Calcite etch pit spreading rates (nm s^{-1}) along (a) [42$\bar{1}$] and (b) [010] directions as a function of HEDP concentration (mM) in solution. The line between data points is plotted as a guide for the eye. The straight lines represent the value in pure water and the dashed lines show the error of these measurements.

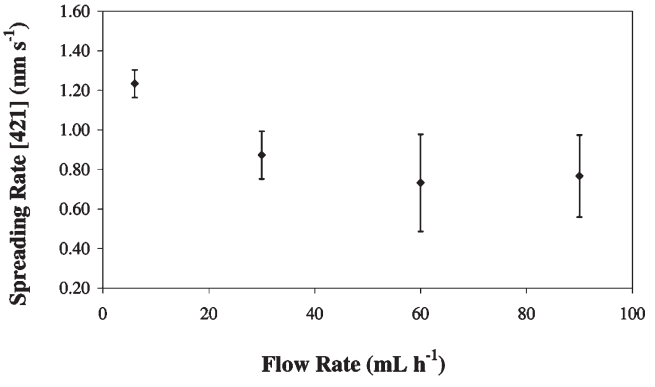

Figure 6. Calcite etch pit spreading rate (nm s^{-1}) along the [42$\bar{1}$] direction in 0.75 mM HEDP solutions (pH 8) as a function of flow rate (mL h^{-1}).

with the observed trend in etch pit spreading rate, thus confirming that the effect of HEDP on calcite dissolution kinetics can be studied from changes in either etch pit spreading rates or macroscopic dissolution rates (i.e., calculated from calcium concentration in AFM outlet solutions). It was also observed that, after the formation of Ca-HEDP precipitates on calcite surfaces due to interaction with 10 mM HEDP solutions (pH = 8), the dissolution rate, after pure water was newly introduced in the fluid cell, was reduced to 3.95×10^{-11} ($\pm 1.47 \times 10^{-12}$), thus indicating that the Ca-HEDP layer protects the calcite surface against further dissolution.

Table 2. Results of Measurement of the Dissolution Rate of Calcite Based on Calcium Flux, R_{mac} (mol cm^{-2} s^{-1}), as a Function of HEDP Concentration

[HEDP] (mM)	R_{mac}	std	log R_{mac}	std
0	2.43×10^{-10}	6.55×10^{-11}	−9.61	0.10
[a]	3.95×10^{-11}	1.47×10^{-12}	−9.94	0.18
0.01	6.22×10^{-11}	2.23×10^{-11}	−10.21	0.12
0.10	2.78×10^{-11}	2.94×10^{-12}	−10.56	0.30
1	8.44×10^{-11}	$2{,}94 \times 10^{-12}$	−10.07	0.07
5	5.18×10^{-10}	5.88×10^{-12}	−9.29	0.04
10	8.03×10^{-10}	8.82×10^{-12}	−9.10	0.08

[a] Dissolution rate in water measured after passing a 10 mM HEDP solution (pH 8) over the calcite cleavage surface during 20 min.

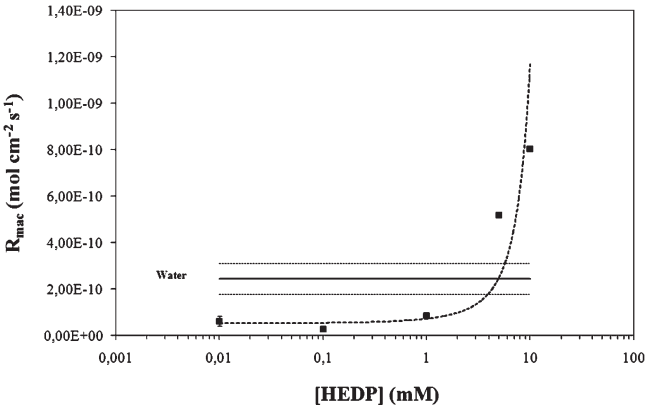

Figure 7. Macroscopic dissolution rates R_{mac} vs concentration of HEDP (rates derived from ICP-OES analyses of [Ca^{2+}] in effluent solution after 20 min AFM dissolution experiments). The line between data points is plotted as a guide for the eye. The straight line represents the value of the dissolution rate in pure water and the dashed lines show the error of this measurement.

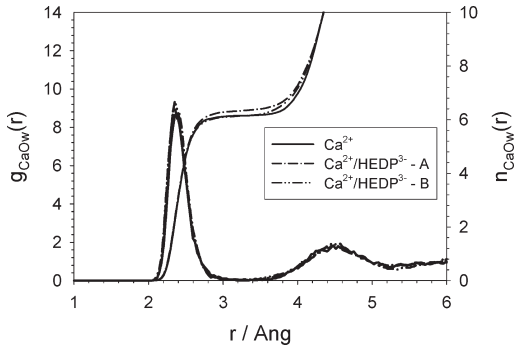

Figure 8. Radial distribution functions, $g(r)$, and running coordination number, $n(r)$, of the Ca−O_w pair obtained from the CP-MD simulations of Ca^{2+} and non-associated Ca^{2+}/$HEDP^{3-}$ pair in water.

(d). Car−Parrinello Molecular Dynamics Simulations: Effect of the $HEDP^{3-}$ on the Structure and Dynamics of Ca^{2+} Hydration Shell. In this section, we discuss the structural properties of the hydration shell of the calcium ion as obtained from the CP-MD simulations of the isolated calcium ion and of the non-associated Ca^{2+}/ $HEDP^{3-}$ pair in water. Figure 8 displays the radial distribution functions (RDFs), $g_{CaOw}(r)$, of the Ca−O_w pair (O_w represents the oxygen atoms of the water molecules), together with the running coordination number,

$$n_{CaO_w}(r) = \frac{4\pi N}{V}\int_o^r g_{CaO_w}(r')\,dr'$$

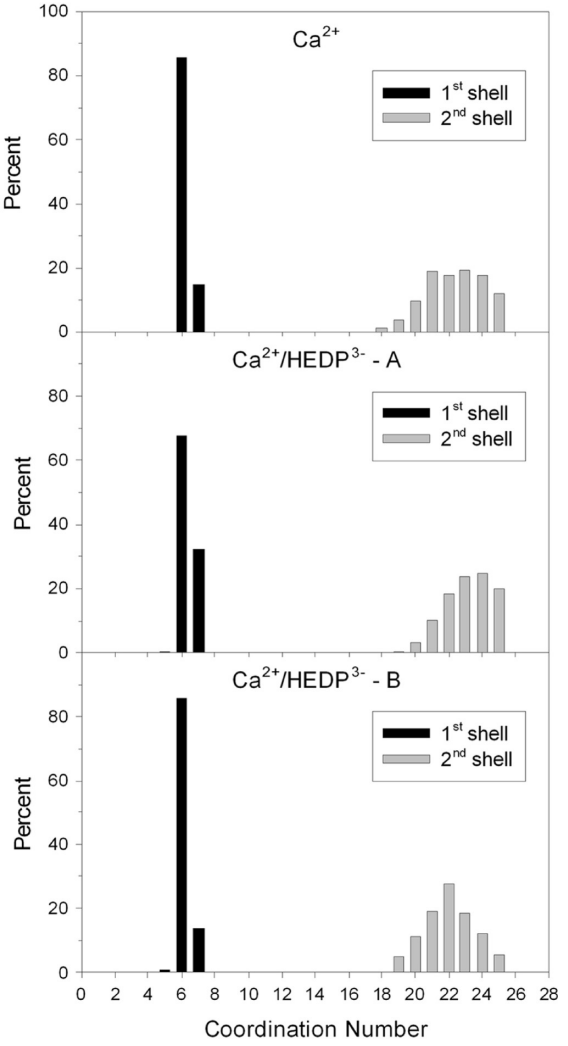

Figure 9. Probability distributions of the hydration numbers of the first coordination shell of the Ca^{2+} obtained from the CP-MD simulations of Ca^{2+} and non-associated Ca^{2+}/$HEDP^{3-}$ pair in water.

where N is the number of oxygen atoms and V is the volume of the simulation cell. The value of $n_{CaO_w}(r)$ at the first minimum of $g_{CaO_w}(r)$ gives the average number of water molecules which are part of the first coordination shell of calcium.

For the isolated Ca^{2+} in water, the integration of the Ca−O_w RDF at 3.2 Å gives an average of 6.1 water molecules coordinated to the metal ion, in agreement with previous first principles MD simulations.[34,35] The Ca−O_w RDFs obtained from two simulations of Ca^{2+}/ $HEDP^{3-}$ in water do not substantially differ from the profile obtained for the isolated Ca^{2+} in water. However, if we compare the profiles of the running coordination number n_{CaO_w} then the first hydration shell of calcium in the Ca^{2+}/$HEDP^{3-}$ aqueous solution obtained from simulation A (6.3) is larger than the first hydration shell of the isolated calcium ion (6.1). However, the profile of $n_{CaO_w}(r)$ obtained from simulation B of Ca^{2+}/$HEDP^{3-}$ does not substantially differ from the profile of Ca^{2+} in water.

The effect of $HEDP^{3-}$ on the hydration structure of calcium can be appreciated better by considering the probability distributions of the first and second hydration shells of Ca^{2+} (Figure 9). We note that on going from the isolated Ca^{2+} ion to the Ca^{2+}/$HEDP^{3-}$ pair in simulation A, the

percentage of seven-coordinated Ca−H_2O complexes in solution increases significantly, from 14 to 32%. This indicates that the presence of $HEDP^{3-}$ in solution may affect the first hydration shell of calcium and therefore its ability to coordinate to other molecules in solution. However, from simulation B we obtain the same population of six- and seven-coordinated Ca−H_2O complexes as found for the isolated Ca^{2+} in water. In order to understand the different results for Ca^{2+}/$HEDP^{3-}$ obtained from the simulations A and B, we report in Figures 10 and 11 the RDF and the time evolution of the Ca−O_p pair, respectively, where O_p represents the oxygen atoms of the diphosphonate molecule. Figure 10 suggests that the diphosphonate molecule never coordinates the calcium ion throughout the CP-MD simulations A and B, and that the oxygen atoms of $HEDP^3$ are part of the second coordination sphere of calcium. In Figure 11, the horizontal dashed line at 3.2 Å defines the coordination limit of the first hydration shell of Ca^{2+}, that is, the position of the first minimum of $g_{CaOw}(r)$ in Figure 8, and the time evolution of d(Ca-O_p) indicates that during simulation A the oxygen atoms O_p are generally closer to calcium than in simulation B.

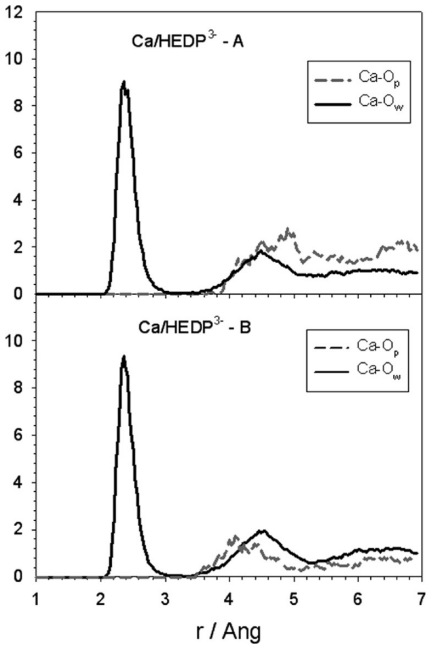

Figure 10. Radial distribution functions, $g(r)$ of the Ca−O_w Ca−O_p pairs for the non-associated Ca^{2+}/$HEDP^{3-}$ pair in water obtained from the CP-MD simulations A and B.

In Table 3, we report the number of exchange events of the water ligands ($N_{ex}^{H_2O}$) in the first and second coordination shells of the calcium ion obtained from the CP-MD simulations of the Ca^{2+} ion and of the Ca^{2+}/$HEDP^{3-}$ pair in water. Table 3 also lists the number of exchange events normalized to 10 ps, $N_{ex}^{H_2O}$/10 ps, which represents a measure of the "lability" of the calcium hydration shell; that is, the higher the number, the more "labile" is the hydration sphere,[30] and the mean residence time (MRT) of water molecules in a given coordination sphere, which can be calculated as

$$\mathrm{MRT} = \frac{t_{\mathrm{sim}} CN_{\mathrm{av}}}{N_{\mathrm{ex}}} \qquad (2)$$

In eq 2, t_{sim} is the simulation time, CN_{av} is the average coordination number, and N_{ex} is the number of accounted exchange events.

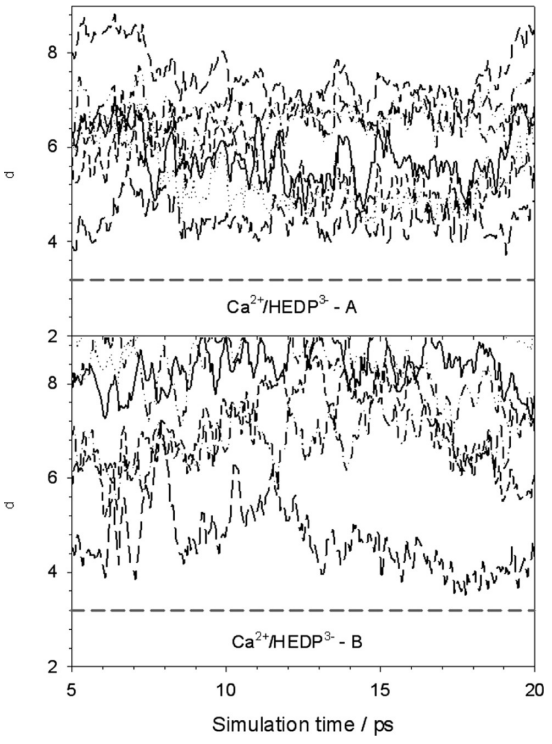

Figure 11. Time evolution of the Ca−O_p distance during simulations A and B of the Ca^{2+}/$HEDP^{3-}$ pair in water. The horizontal dashed line at 3.2 Å defines the first hydration shell of the calcium ion.

Table 3. Number of Accounted Water Exchange Events ($N_{ex}^{H_2O}$) in the First and Second Coordination Shells of the Calcium Atom, with a Duration of More than $t > t^*$, Obtained from the CP-MD Simulations of the Ca^{2+} Ion and of the Non-Associated Ca^{2+}/HEDP Pair in Water[a]

			$t^* = 0.5$ ps		
	CN	t_{sim}	$N_{ex}^{H_2O}$	$N_{ex}^{H_2O}$/10 ps	MRT (ps)
1st shell					
Ca^{2+}/83 H_2O	6.1	19.5	4	2.1	29.7
Ca^{2+}/HEDP/77 H_2O − simulation A	6.3	19.9	6	3.0	20.9
Ca^{2+}/HEDP/77 H_2O − simulation B	6.1	20.0	4	2.0	30.5
2nd shell					
Ca^{2+} (QM/MM)[b]	19.1	21.8	94	43.1	4.4
Ca^{2+}/83 H_2O	22.8	19.5	74	37.9	6.0
Ca^{2+}/HEDP/77 H_2O − simulation A	21.5	19.9	75	39.1	5.7
Ca^{2+}/HEDP/77 H_2O − simulation B	21.3	20.0	70	35.0	6.1

[a] The first and second coordination shells have been defined by the coordination limits r(Ca−O) = 3.2 Å and r(Ca−O) = 5.5 Å, respectively. [b] Ref 30.

The results obtained for simulation A of Ca^{2+}/$HEDP^{3-}$ in water suggest that the presence of the $HEDP^{3-}$ in solution increases the "lability" of the first hydration shell, with an estimated additional water exchange process every 10 ps compared to the isolated Ca^{2+} (see Table 3). Moreover, our simulations indicate that the MRT of water molecules in the first hydration shell of calcium decreases by almost one-third, from 29.7 to 20.9 ps, when $HEDP^{3-}$ is present in solution. On the other hand, the number of exchange events in the first hydration shell of calcium encountered during simulation B is the same as the one obtained for the simulation of isolated Ca^{2+} in water. Note, however, that in simulation B the average $d(Ca-O_p)$ distances are larger than in simulation A (see Figure 11). Because the first principles molecular dynamics simulations reported in the present study are extremely time-consuming (approximately 7000 core hours to perform 5 ps), we were limited to very short simulation times which could possibly be statistically inadequate to firmly support the conclusion that a HEDP molecule could increase the lability of the calcium hydration shell. However, Table 3 also reports the number of water exchange events in the second hydration shell of calcium. In this case, the effect of the diphosphonate molecule is negligible, as a MRT of approximately 6 ps is computed from all three simulations. This consistency indicates the reproducibility of our simulations and therefore the values of MRT obtained for the first hydration shell of calcium. Moreover, the number of exchange events $N_x^{H_2O}$/10 ps and MRT of the second shell of Ca^{2+} obtained from the CP-MD simulations are in very good agreement with the results obtained by Hofer et al.[30] using QM/MM simulations at the Hartree−Fock level of theory.

Discussion

(a). Effect of Phosphonates on Dissolution Rates and Nucleation Density: Changes in the Dynamics of Calcium Hydration and Surface Hydration Water. Our results show that the presence of HEDP in solution results in a drastic decrease in calcite dissolution rates. An important effect, discussed in more detail in the next section, is HEDP adsorption on calcite surface sites. Molecular simulations have shown that HEDP probably adsorbs to pairs of calcium sites in obtuse (+) steps.[15] This hampers the movement of such steps, thereby reducing etch pit spreading rates. HEDP adsorption into calcite obtuse steps at low concentration results in the observed reduction in the dissolution rates compared with those measured in pure water.

However, increasing the HEDP concentration leads to the observed enhancement of etch pit spreading rates. This trend differs from that observed by Kanellopoulou and Koutsoukos,[19] who found a continuous decrease in calcite dissolution rate with increasing HEDP concentration. However, these results refer to a polycrystalline material and represent all possible calcite faces. Furthermore, their experiments were conducted in the presence of 0.1 M NaCl, and we have evidence that the presence of Na^+ results in the precipitation of a Ca−Na−HEDP phase which may hinder calcite dissolution (unpublished results). Our AFM flow-through experiments were performed with a semicontinuous flow. Solution was injected into the fluid cell, left static during picture capture (approximately 1.5 min) and then fresh solution was again injected. Thus, although equilibrium between the solid and the fluid is not expected to be reached, the formation of complexes in solution may have some influence on dissolution kinetics. At low flow rates (i.e., 6 mL h^{-1}), calcite dissolution cannot be considered as surface or reaction controlled. Then, the formation of Ca-HEDP complexes in solution results in a reduction in the calcium-free activity in solution. This leads to an increase in the solubility of calcite, thereby increasing the driving force for dissolution and, as a consequence, increasing the dissolution rate. This explains why dissolution rates measured at high flow rate (i.e., 60 mL h^{-1}) are systematically lower for all HEDP concentrations tested than those observed at low rates. However, at flow rates higher than 60 mL h^{-1}, the kinetics of dissolution is independent of the flow rate, which indicates that this effect is no longer controlling the kinetics of dissolution.

We also considered a hypothetical effect of the formation of surface complexes on dissolution kinetics. Although our AFM set up does not allow monitoring of the surface speciation during the experiments within the fluid cell, this can be inferred by modeling. Surface complexation model of calcite postulates the formation of the two primary hydration sites, $>CaOH^0$ and $>CO_3H^0$ (where $>$ represents the surface site of the mineral lattice) having a 1:1 stoichiometry on the cleavage surface exposed to the aqueous solution.[36] Protonation and deprotonation reactions of these primary sites as a function of the pH are responsible for the charge of the calcite surfaces. Such a thermodynamic model of the carbonate/solution interface was initially derived from the results of macroscopic techniques (surface titration, electrokinetics, and dissolution rate studies) and further confirmed at the microscopic scale (diffuse reflectance infrared spectroscopy).[37] Surface complex formation correlates with the equilibrium formation of the corresponding complexes in solution. We modeled aqueous solution as well as surface complexes concentrations using PHREEQC[38] (Figure 12). The values of stability constants of HEDP complexes in solution and protonation constants used in this modeling (not included in the phreeqc.dat database) are those reported in Popov et al.[39] and Deluchat et al.[40] (see Table 4). The strength of surface complexes can be inferred by analogy with the comparable aqueous complexes.[41] This approach has been followed also for the case of aspartate molecules interacting with calcite surfaces.[17] At the pH of the experiments and in the absence of Ca^{2+}, HEDP is mainly present in solution as $HEDP^{3-}$ (93.4%) (Figure 12a). Free HEDP (i.e., not forming complexes in solution) may bind to calcium sites in calcite cleavage planes forming surfaces complexes which modify the reactivity and the hydration environment of calcium sites. The hydration reaction of surface Ca^{2+} cations is given by the equation

$$>Ca^+ + H_2O \rightarrow >CaOH^0 + H^+ \qquad \text{(Reaction 1)}$$

In the presence of HEDP, the formation of the following complexes on the calcite surface is possible:

$$>Ca^+ + HEDP^{4-} \rightarrow >Ca\text{-}HEDP^{3-} \qquad \text{(Reaction 2)}$$

$$>Ca^+ + HEDP^{3-} \rightarrow >Ca\text{-}HEDP^{2-} \qquad \text{(Reaction 3)}$$

$$>Ca^+ + CaHEDP^{2-} \rightarrow >Ca\text{-}HEDP\text{-}Ca^- \qquad \text{(Reaction 4)}$$

The pK values for these reactions, inferred for the corresponding equilibrium constant in solution, are −12.78, 6.4, 3.3, and 4.6, respectively. Therefore, it is clear that Ca-HEDP complexes will be predominant surface species when HEDP is

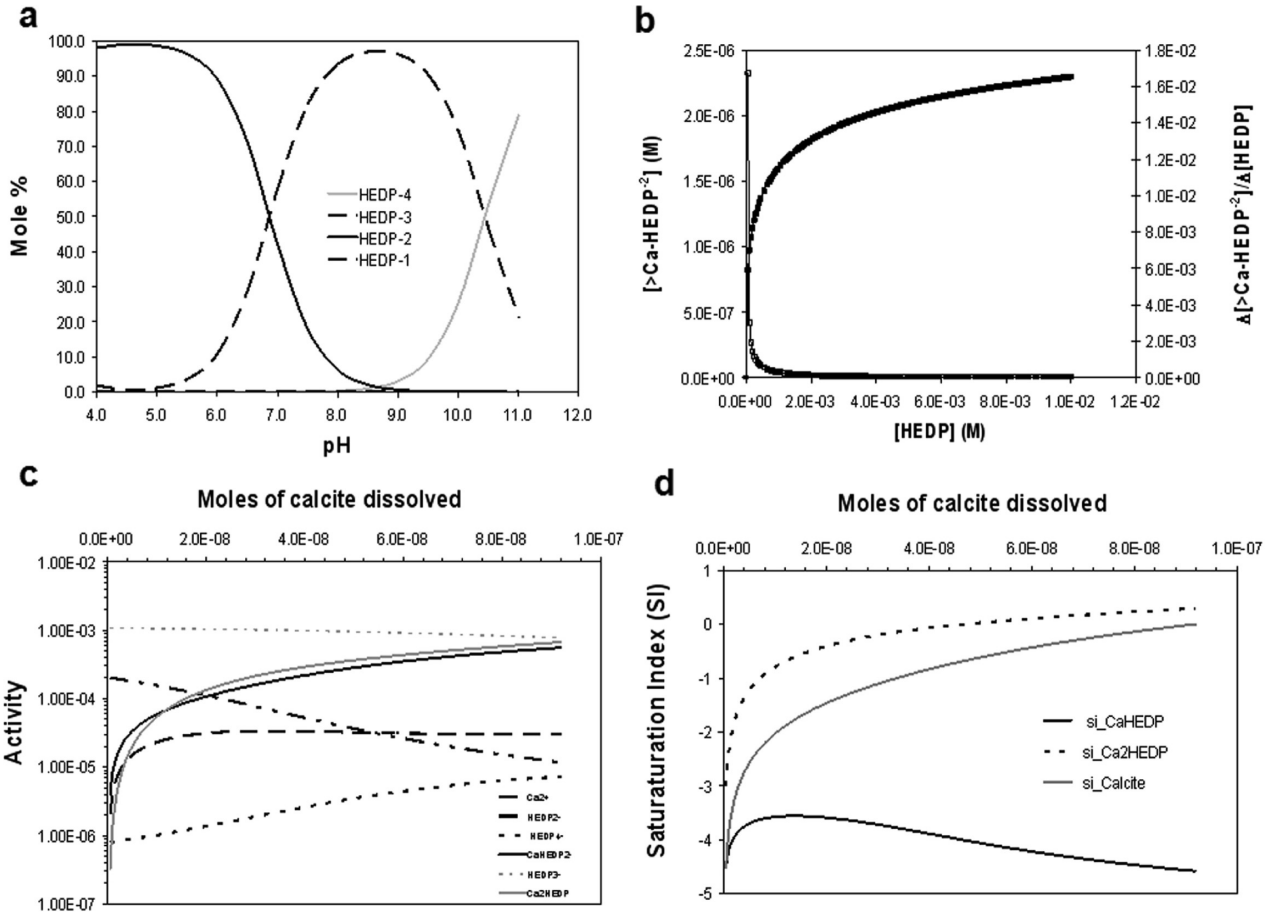

Figure 12. (a) HEDP speciation as a function of pH and (b) [> Ca-HEDP^{2-}] surface concentration (■) and its variation (□) as a function of HEDP concentration in solution. Results of the PHREEQC modeling of the evolution of a hypothetical batch reaction in the AFM fluid cell of calcite with a 5 mM HEDP aqueous solution (pH 8): (c) solution speciation and (b) saturation indices (SI) of calcite, CaHEDP, and Ca_2HEDP as a function of moles of calcite dissolved.

present in solution. The concentration of >Ca-HEDP^{2-} complexes (which was found to be the most abundant surface species under our experimental conditions) is plotted in Figure 12b as a function of HEDP in solution (at pH 8). Little changes in the concentration of >Ca-HEDP^{2-} occur for [HEDP] > 1 mM, which is when we found the highest increase in the dissolution rate. Thus, this effect alone cannot explain why calcite dissolution rates increase drastically at concentrations above 1 mM and high flow rate (60 mL h^{-1}), when the amount of surface Ca-HEDP complexes is not substantially modified upon increasing the HEDP concentration.

Another aspect that is not very frequently considered during mineral dissolution and growth studies is the fact that ions or molecules present in solutions in contact with minerals can alter the solvation environment of the building units of a crystal and consequently change the kinetics of dissolution and growth processes. For example, recent results[42,43] have shown that mineral nucleation and growth, as well as dissolution, are strongly affected by changes in the solvation environment induced by inorganic compounds present in solution. Ions in aqueous solutions are surrounded by a solvation layer of water molecules, more or less tightly bound depending on the ion size and charge (i.e., in the surface charge density), and one of the most important features for the reactivity of ions in solution is the process of releasing a ligand in order to coordinate to another, either similar or a different kind.[44] Solvation of the cation is assumed to be the rate limiting step for dissolution of calcite, as suggested by Pokrovsky and Schott[45] for divalent carbonates and by Dove and Czank[46] for divalent sulfates. The

Table 4. Solubility Products (log K_{sp}) of Ca-HEDP Calculated Using Data from Browning and Fogler (1996) and Equilibrium Constants Used in the Modelling of the Ca-HEDP Aqueous Solution Speciation[a]

Solubility Products	
Ca-HEDP	−4.35
Ca_2-HEDP	−12.68
Protonation Constants	
log K_1[b]	11.0
log K_2[b]	6.9
log K_3[b]	2.7
log K_4[b]	1.6
Complexation Constants	
	log K
M + L → ML[c]	6.4
M + HL → MHL[c]	3.3
M + ML → M2L[c]	4.6
M + L + 2H$^+$ → MH2L[b]	21.83
M + L + H$^+$ → MHL[b]	14.2
ML + H$^+$ → MHL[b]	8.16
MHL + H$^+$ → MH2L[b]	7.63

[a] M = Ca^{2+}; L = $HEDP^{4-}$. [b] Ref 49. [c] Ref 48.

presence of foreign organic and/or inorganic species could influence the frequency of water molecule exchange in the hydration shell of a metal, and therefore its reactivity.

We chose two different initial configurations for MD simulations (A and B) to verify the hypothesis that diphosphonate molecules in solution could affect the reactivity of the calcium ion not only through the mechanism of metal complexation, but also because of possible effects of $HEDP^{3-}$ on the structural and dynamical properties of the first hydration shell of Ca^{2+}. In fact, in both simulations A and B the diphosphonate molecule was never coordinated to the calcium ion (see Figures 9 and 10), and the influence of the organic molecule could be explained in terms of modification of its neighboring water molecules, and consequent "reconstruction" of the hydration shell of the calcium ions. Our CP-MD simulations of the $Ca^{2+}/HEDP^{3-}$ pairs in water indicate that the diphosphonate molecule affects both the structure and the dynamics of the water molecules around the cation. Moreover, the differences found between the two sets of simulations A and B suggest that the perturbation of the hydration sphere of the calcium ion, which consequently affects its ability to coordinate to other molecules in solution, depends on the average distance between the calcium ion and the chelating oxygen atoms of the diphosphonate molecule. The average $Ca-O_p$ distances decrease as the concentration of diphosphonate in solution increases. Our simulations therefore suggest that at high concentrations of HEDP the rates of calcium carbonate dissolution/precipitation are affected not only by processes of calcium complexation but also because of the perturbation of the dynamic and structural properties of the calcium hydration shell by the noncoordinated organophosphonate molecules present in solution.

Our CP-MD simulations indicate that the presence of $HEDP^{3-}$ in solution can decrease the mean residence time of the water molecules in the first hydration shell of calcium and consequently modify the reactivity of Ca^{2+}. Increasing water exchange around calcium ion in solution should in principle hamper calcite dissolution. However, due to its relatively small radius and high charge, Ca^{2+} hydration during dissolution causes significant ordering in the solvent molecules attracted by the ion, compared to bigger divalent cations such as Ba^{2+}, as deduced from the values of entropies of solvation of calcium and barium ($\Delta S_{str} = -40\ J\ mol^{-1}\ K^{-1}$ and $-10\ J\ mol^{-1}\ K^{-1}$, respectively), that are due solely to the interaction of an ion with the water in its environment.[47] Thus, with increasing frequency of water exchange between the bulk solution and the calcium hydration shell, the negative entropic effect of Ca^{2+} hydration upon calcite dissolution is reduced and, as a consequence, dissolution is enhanced.

In summary, the overall etch pit spreading rate will be determined mainly by both HEDP adsorption on obtuse steps and blocking of etch pit spreading, and the effect of $HEDP^{3-}$ on the hydration shell of calcium, which depends on the concentration of HEDP in solution. In general, we can say that the presence of organic molecules, which increases water exchange between the calcium hydration shell and the bulk solution, results in an increase in the calcium dissolution rate due to a decrease in a negative entropic effect upon calcite dissolution. However, for cations with a lower charge density than Ca^{2+}, this will not be the case, and the increase in the frequency of water exchange will lead to a decrease in ion hydration, which reduces the dissolution rate. As an example, we can cite the case of barite dissolution in the presence of DTPA.[48,49] These authors found that increasing DTPA concentration led to a reduction in the dissolution rate of barite, that is, increasing DTPA concentration makes the solution a less effective solvent for barite.

Desolvation of the surface may also represent an important energetic barrier for dissolution. Many experimental and computational studies have revealed that crystal surfaces cause an ordered and tightly bound layer of water molecules to be present on the surface. Fenter et al.[50] showed, by using X-ray reflectivity measurements, the presence of a monolayer of hydroxyl species adsorbed on calcite cleavage surfaces. Computational studies also demonstrated the presence of a strongly bound water layer on calcite and on other solids.[51−55] This layer provides an effective activation barrier to dissolution. It is known that desolvation of mineral surfaces may be aided by the presence of some ions that are able to disrupt the surface hydration layer, and therefore increase mineral dissolution rates.[56] The PO_3^{2-} groups in phosphonate molecules make them highly hydrophilic molecules. HEDP physisorption on calcite surfaces and subsequent competition for hydrating water may cause a reduction in the energy barrier for 2D nucleation of an etch pit due to the surface destabilization associated with the disruption of the calcite surface hydration layer. This can explain the observed increase in etch pit density found in the presence of HEDP.

(b). Effect of Phosphonates on Etch Pit Morphology. AFM observations on etch pit formation and propagation during dissolution processes have shown that the presence of phosphonates considerably modifies the morphology of etch pits developed on calcite cleavage surfaces. The usual rhombohedral etch pits observed on calcite surfaces during dissolution in pure water were changed to tear-shaped or pentagonal (see Figures 1 and 2). Our observations are in agreement with the results of previous studies of calcite growth and dissolution in the presence of phosphonates, reporting also morphology changes.[13,18] These changes were explained by considering the adsorption of HEDP molecules to calcite steps.[15] As already mentioned, Nygren et al.[15] explored HEDP−calcite interactions by molecular modeling, and concluded that the observed behavior may be explained by considering bidentate adsorption of HEDP molecules to pairs of calcium sites in obtuse (+) steps. This hampers the movement of the kinks and antikinks along such steps, thereby reducing etch pit spreading rates and changing the morphology of the etch pits. This is in agreement with the etch pit morphology observed in our AFM experiments, in which pinning of the +/+ corner can be detected (Figure 1). However, a detailed observation of the morphology changes induced by the presence of phosphonates also reveals the development in the etch pits of step edges parallel to $[4\bar{2}1]$ (Figure 2). These directions correspond to the intersection of the $\{01\bar{1}2\}$ form with the cleavage rhombohedron. The $(01\bar{1}2)$ and (0001) faces are polar and consist of alternate layers of Ca^{2+} and CO_3^{2-} ions in successive planes. Thus, they are not stable under normal growth conditions (i.e., nucleation from pure solutions). However, both are frequently observed when nucleation and growth occur in the presence of organic molecules (see the work by Duffy and Harding[57] and references therein). In fact, the (0001) face is the most commonly found orientation in biomineralized calcite. This general feature of calcite grown in the presence of a wide range of organic molecules, with different functional groups and molecular structures, suggests that the effect of organics on

calcite morphology is not due solely to specific recognition and structural matching between organic molecules and calcite active growth sites. The formation of Ca-phosphonate surface species may reduce repulsive interactions between like-charges and reduce attractive interactions between unlike charges. Thus, polar faces will be stabilized while nonpolar faces, which are stable under normal growth conditions, should be less stable when phosphonate species bind to calcium ions on the surface. The stronger the binding, the larger the stabilization of polar faces will be and so its impact on mineral growth and dissolution morphology. In this sense, Didymus et al.[58] found that the effect of phosphonates on calcite growth morphology decreases with decreasing hydrophilicity of the molecule, thus indicating that the effect of additives depends not only on the charge of the molecule but also on its spatial charge distribution. For the same charge, smaller ions can get closer to the solute atoms, resulting in stronger binding. Thus, we hypothesize here that the presence of HEDP may neutralize the dipole moment of polar faces, which results in $(01\bar{1}2)$ stabilization during calcite dissolution. As already mentioned, this is reflected in changes in the morphology of etch pits formed on calcite cleavage surfaces during dissolution in the presence of HEDP.

(c). Precipitation Processes during the Interaction of Calcite Surfaces with HEDP Aqueous Solutions. In our experiments at high phosphonate concentration (> 5 mM), the reaction of a calcite surface with HEDP follows a pathway of dissolution of the substrate followed by precipitation of a calcium phosphonate phase. This layer passivates the calcite surface, which decreases the dissolution rate. During the interaction, the release of Ca^{2+} and CO_3^{2-} ions from the dissolving calcite to the solution occurred simultaneously with the reaction between Ca^{2+} and HEDP to form a CaHEDP precipitate according to the reaction:

$$HEDP^{2-}\ (\text{aqueous}) + CaCO_3\ (\text{solid}) \leftrightarrow CaHEDP\ (\text{solid}) + CO_3^{2-}\ (\text{aqueous}) \qquad \text{(Reaction 5)}$$

This reaction is important in the oil industry where phosphonates are used as scale inhibitors. The formation of calcium-phosphonate precipitates may be a troublesome deposit in oil pipes and can also deplete the solution concentration to such an extent that calcium carbonate scales appear.[59] However, precipitation of Ca-phosphonate phases in carbonate reservoirs has been proposed as a way of slowly releasing the compound for the inhibition of calcite scale formation from porous media.[6] Precipitation of layered calcium phosphonate compounds that bind to the surface of cement grains, thus inhibiting their hydration, has been described as the most probable mechanism by which phosphonates delay cement hydration.[60] Activities of different chemical species and saturation indexes (SI) with respect to Ca-phosphonate phases were calculated using PHREEQC.[38] The saturation index is defined as

$$SI = \log\left(\frac{IAP}{K_{sp}}\right) = \log\left(\frac{a_{Ca^{2+}} a_{HEDP^{2-}}}{K_{sp}}\right) \qquad (3)$$

where $a_{Ca^{2+}}$ and $a_{HEDP^{2-}}$ are Ca^{2+} and $HEDP^{2-}$ ion activities, respectively, and K_{sp} is the solubility product of the solid phase considered. Values of solubility products of calcium phosphonate phases were not available in the PHREEQC database, so data found in the literature was used to calculate these constants and they were introduced into the model of the system (Table 4). The hypothetical evolution of the solution composition within the fluid cell in a batch reaction (for an initial HEDP concentration of 5 mM) and SI with respect to CaHEDP and Ca_2HEDP (simulated using PHREEQC) are shown in Figures 12, panels c and d respectively. As can be seen, the solution is undersaturated with respect to the crystalline phase, $Ca(CH_3C(OH)(PO_3H)_2)\cdot 2H_2O$, which is the one that precipitates until the equilibrium with respect to calcite is reached. However, in our flow-through set up equilibrium would not be reached, and this concentration is used just as a reference for the maximum or threshold value in our experiments. If the initial amount of calcite dissolved mixes with the bulk solution, thermodynamic calculations indicate undersaturation with respect to $Ca(CH_3C(OH)(PO_3H)_2)\cdot 2H_2O$; however, this is not the case as precipitation of this Ca-HEDP phase was observed. Nevertheless, if the dissolution of the substrate occurs faster than the fluid phase can equilibrate by diffusion, the fluid at the interface may be immediately supersaturated with respect to a Ca-HEDP phase that precipitates. Thus, our experimental results suggest that this coupled dissolution−precipitation reaction is controlled by the fluid composition in a boundary layer at the interface with the solid substrate, which has a different composition to the fluid in the bulk. This is a general feature of mineral replacement reactions.[61] The fluid−solid equilibrium between the solution and the parent solid is only maintained within this layer, whose thickness depends on the relative dissolution rate of the parent crystal, the epitaxial nucleation of the product crystal and the mass transport rate through the fluid to the reaction interface.[62] The precipitation of such a phase occurs simultaneously, or is coupled to further calcite dissolution. The presence of this boundary layer may also have implications for the interpretation of calcite dissolution rates. The formation of the calcium phosphonate phase depleted the free calcium concentration in this layer, and therefore this may contribute, to some extent, to the observed increases in dissolution rate at HEDP concentration > 5 mM. The growth of the product seems to be crystallographically controlled or oriented by the structure of the underlying crystal, which indicates some degree of structural matching or epitaxy between the parent and the product phases. Possible epitaxial relationships will be explored in the next section.

(d). Structural Relationships between Calcite and Ca-Phosphonate Overgrowth. As already shown, the composition of the overgrowing islands can be assumed to be the crystalline 1:1 compound. The crystal structure of CaHEDP has been determined by Uchtmann.[33] $Ca(CH_3C(OH)(PO_3H)_2)\cdot 2H_2O$ crystallizes in a triclinic unit cell, space group $P\bar{1}$; the reduced cell parameters are $a' = 6.961(3)$, $b' = 7.625(4)$, $c' = 9.729(4)$ Å, $\alpha' = 92.52(7)°$, $\beta' = 106.08(7)°$, $\gamma' = 112.85(5)°$. The structure forms a network of infinite 2D layers parallel to the (001) plane (see Figure 13a). The morphology of the crystals was simulated using SHAPE software (Figure 13b). From the very early stages, the islands were three-dimensional, with a constant thickness of 4 monolayers along the [001] direction. The growth of the product occurred by spreading of these multilayer islands, which appears to be energetically more favorable than the advancement of monolayers on a substrate of different composition. This behavior is in agreement with a Volmer−Weber mechanism of epitaxy.[63] This mechanism is observed when there is a weak adhesion between substrate and overgrowth, and suggests the existence of a nonfully coherent substrate−overgrowth interface.[64] If the

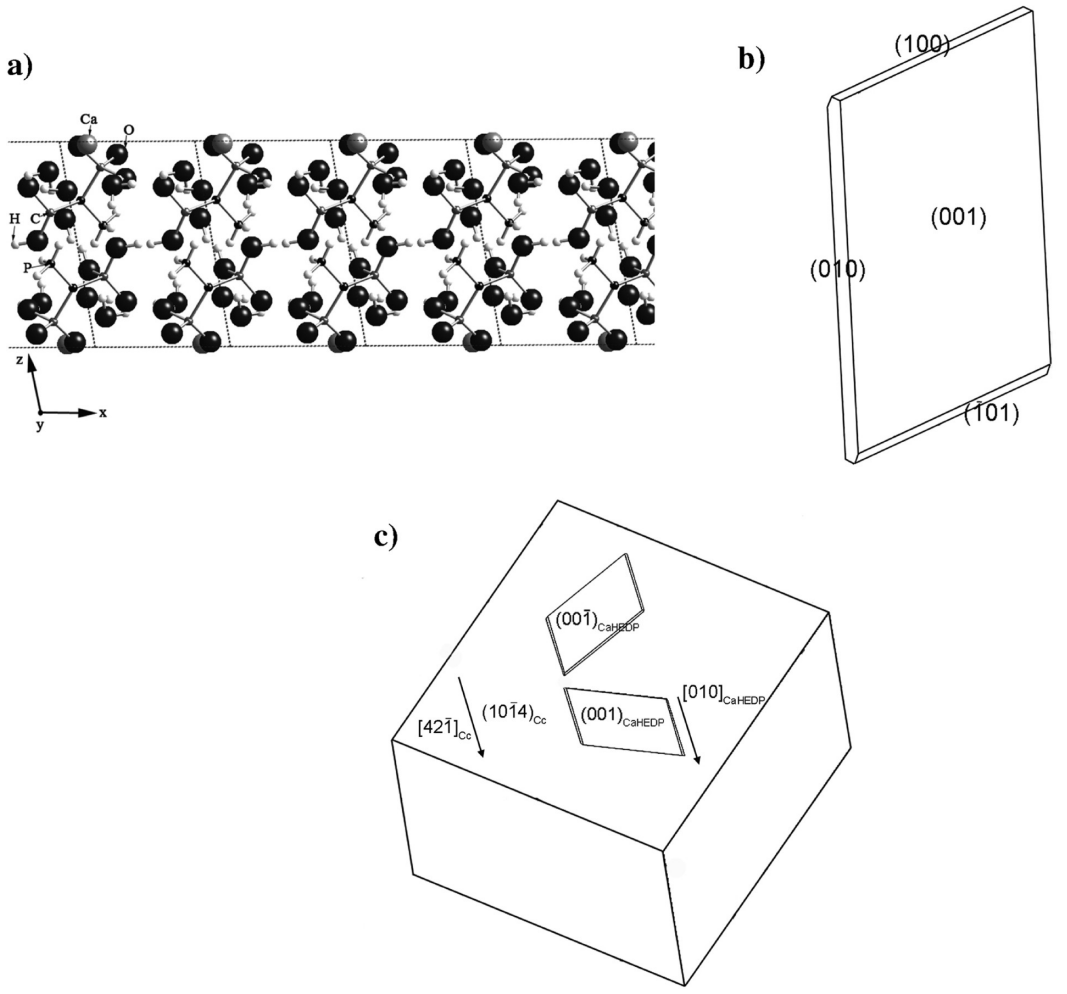

Figure 13. (a) Layered CaHEDP structure on the (010) plane (fractional atomic coordinates from Utchmann 1972). (b) CaHEDP morphology and (c) epitaxial relationship with calcite simulated using SHAPE software.

crystallographic matching between the parent calcite and overgrowth is not high, the product may have a significant level of intrinsic stress and will tend to reduce this stress via the formation of a free surface normal to the growth layer (i.e., by forming thick 3D nuclei instead of monolayers). The fact that growth initially stops at the edges of calcite etch pits, reproducing the topography of the parent solid (i.e., template effect[65]), also indicates a crystallographic mismatch between the substrate and the overgrowth. The structural misfit (mf) can be calculated using the equation:[66]

$$\text{mf}\ (\%) = \frac{2(t_{[\text{uvw}]\text{Cc}} - t_{[\text{uvw}]\text{CaHEDP}})}{t_{[\text{uvw}]\text{Cc}} + t_{[\text{uvw}]\text{CaHEDP}}} \qquad (4)$$

where $t_{[\text{uvw}]}$ is the repeating period along the [uvw] direction in calcite (Cc) and CaHEDP. For (001) CaHEDP and (10$\bar{1}$4) calcite faces we observed a very good match along $[010]_{\text{CaHEDP}}$ and $[42\bar{1}]_{\text{Cc}}$, with a misfit of only 0.12%. However, the simultaneous match along other equivalent directions on these planes is not so good. If we compare the repeating periods of calcite and CaHEDP along [$\bar{4}$41] and [100], respectively, we obtain a misfit of about −8%. There is an angular misfit of about 9.4°. The proposed epitaxial relationship is shown in Figure 13c. These observations suggest that the reticular control could be essentially one-dimensional, with $[42\bar{1}]_{\text{Cc}}$ and $[010]_{\text{CaHEDP}}$ as the corresponding directions.

Conclusions

The presence of an organic disphosphonate (HEDP) in a solution in contact with calcite surfaces resulted in changes in both the appearance and the spreading rates of the dissolution features developed on cleavage surfaces with respect to those observed in the presence of pure water. Adsorption of HEDP on obtuse steps of calcite surfaces can partially explain the observed changes in surface topography and the decrease in the etch pit spreading rate at low HEDP concentration. Additionally, the presence of HEDP may help to neutralize the dipole moment of polar (01$\bar{1}$2) faces, non stable under normal growth conditions, which results in the observed development within the etch pits of step edges parallel to [4$\bar{2}$1]. First principles molecular dynamics simulations have shown that the presence of diphosphonate molecules in solution increases the hydration sphere of calcium and the frequency of exchange of the water molecules in the first hydration shell of the calcium ion. This may counteract the negative entropic effect of calcium hydration occurring upon calcite dissolution, resulting in an increased dissolution rate with HEDP concentration in solution.

Additionally, the nucleation and growth of a new phase, identified as $Ca(CH_3C(OH)(PO_3H)_2)\cdot 2H_2O$, on calcite surfaces was observed, although the bulk solution was undersaturated with respect to this calcium HEDP phase. This gives

indirect evidence for the existence of a boundary layer at the carbonate−fluid interface, whose composition controls the interaction between the solid and the solution. During calcite dissolution, the release of calcium to this boundary layer leads to its supersaturation with respect to CaHEDP, which immediately precipitates. This phase seems to precipitate with its (001) face parallel to calcite cleavage surfaces, possibly with the $[010]_{CaHEDP}$ direction aligned parallel to $[42\bar{1}]_{Cc}$. The results of this research have shed some light on the mechanisms of the interaction between minerals and organic molecules, which may be of interest in a wide range of fields, including medicine, biomineralization, and the oil and cement industry. Moreover, this work represents a source of information that may help in the design of new conservation treatments for ornamental and building stone based on the in situ formation of functional organic films that reduce solution-induced weathering of stone via nanofilm formation at the mineral/solution interface.

Acknowledgment. This work is carried out within the EU Initial Training Network Delta-Min (Mechanisms of Mineral Replacement Reactions) Grant PITN-GA-2008-215360, the EU Early Stage Training Network MIR (Mineral-fluid Interface Reactivity) Contract No. MEST-CT-2005-021120 and the EU Research Training Network MIN-GRO Contract No. MRTN-CT-2006-035488. Experimental facilities are supported by the Deutsche Forschungsgemeinschaft (DFG). Computer resources on the UK "HECToR service" were provided via our membership of the UK's HPC Materials Chemistry Consortium (Grant No. EPSRC EP/D504872) and the NERC Computational Mineral Physics Consortium. We are thankful to three anonymous referees for all the constructive comments that have helped us to improve the overall quality of our paper.

References

(1) Morse, J. W.; Arvidson, R. S.; Lüttge, A. *Chem. Rev.* **2007**, *107*, 342–381.
(2) Nowack, B. *Water Res.* **2003**, *37*, 2533–2546.
(3) Jonasson, R. G.; Rispler, K.; Wiwchar, B.; Gunter, W. D. *Chem. Geol.* **1996**, *132*, 215–225.
(4) Nowack, B.; Stone, A. T. *J. Colloid Interface Sci.* **1999**, *214*, 20–30.
(5) Pairat, R.; Sumeath, C.; Browning, F. H.; Fogler, H. S. *Langmuir* **1997**, *13*, 791–798.
(6) Fleisch, H. *Clin. Orthop. Relat. Res.* **1987**, *217*, 72–78.
(7) van der Pluijm, G.; Vloedgraven, H.; van Beek, E.; van der Wee-Pals, L.; Löwik, C.; Papapoulos, S. *J. Clin. Invest.* **1993**, *98*, 698–705.
(8) Fleisch, H. *Breast Cancer Res.* **2002**, *4*, 30–34.
(9) van Poznak, C. H. *Cancer Control* **2002**, *19*, 480–489.
(10) Ruiz-Agudo, E.; Rodríguez-Navarro, C.; Sebastián Pardo, E. *Cryst. Growth Des.* **2006**, *6*, 1575–1583.
(11) Ruiz-Agudo, E.; Putnis, C. V.; Rodríguez-Navarro, C. *Cryst. Growth Des.* **2008**, *8*, 2665–2673.
(12) Ruiz-Agudo, E. *Prevención del daño debido a la cristalización de sales en el patrimonio histórico construido mediante el uso de inhibidores de la cristalización*; Universidad de Granada: Granada, Spain, 2007.
(13) Gratz, A. J.; Hillner, P. E. *J. Cryst. Growth* **1993**, *129*, 789–793.
(14) Reyhani, M. M.; Oliveira, A.; Parkinson, G. M.; Jones, F.; Rohl, A. L.; Ogden, M. I. *Int. J. Mod. Phys. B* **2002**, *16*, 25.
(15) Nygren, M. A.; Gay, D. H.; Catlow, C. R. A.; Wilson, M. P.; Rohlbet, A. L. *J. Chem. Soc., Faraday Trans.* **1998**, *94*, 3685–3693.
(16) Ojo, S. A.; Slater, B.; Catlow, C. R. A. *Mol. Simul.* **2002**, *28*, 591.
(17) Teng, H. H.; Dove, P. M. *Am. Mineral.* **1997**, *82*, 878–887.
(18) Britt, D. W.; Hlady, V. *Langmuir* **1997**, *13*, 1873–1876.
(19) Kanellopoulou, D. G.; Koutsoukos, P. G. *Langmuir* **2003**, *19*, 5691–5699.
(20) Shiraki, R.; Rock, P. A.; Casey, W. H. *Aquat. Geochem.* **2000**, *6*, 87–108.
(21) De Giudici, G. *Am. Mineral.* **2002**, *87*, 1279–1285.
(22) Duckworth, O. W.; Martin, S. T. *Am. Mineral.* **2004**, *89*, 554–563.
(23) Car, R.; Parrinello, M. *Phys. Rev. Lett.* **1985**, *55*, 2471–2474.
(24) Giannozzi, P.; Baroni, S.; Bonini, N.; Calandra, M.; Car, R.; Cavazzoni, C.; Ceresoli, D.; Chiarotti, G. L.; Cococcioni, M.; Dabo, I.; Dal Corso, A.; de Gironcoli, S.; Fabris, S.; Fratesi, G.; Gebauer, R.; Gerstmann, U.; Gougoussis, C.; Kokalj, A.; Lazzeri, M.; Martin-Samos, L.; Marzari, N.; Mauri, F.; Mazzarello, R; Paolini, S.; Pasquarello, A.; Paulatto, L.; Sbraccia, C.; Scandolo, S.; Sclauzero, G.; Seitsonen, A. P.; Smogunov, A.; Umari, P.; Wentzcovitch., R. M. QUANTUM ESPRESSO: a modular and open-source software project for quantum simulations of materials. *J. Phys.: Condens. Matter* **2009**, *21*, 395502–395521.
(25) Perdew, J. P.; Burke, K.; Ernzerhof, M. *Phys. Rev. Lett.* **1996**, *77*, 3865–3868.
(26) Vanderbilt, D. *Phys. Rev. B* **1990**, *41*, 7892–7895.
(27) http://www.physics.rutgers.edu/~dhv/uspp/
(28) Martyna, G. J.; Klein, M. L.; Tuckerman, M. *J. Chem. Phys.* **1992**, *97*, 2635–2643.
(29) Sit, P.H.-L.; Marzari, N. *J. Chem. Phys.* **2005**, *122*, 204510.
(30) Hofer, T. S.; Tran, H. T.; Schwenk, C. F.; Rode, B. M. *J. Comput. Chem.* **2003**, *25*, 211–214.
(31) Astilleros, J. M.; Pina, C. M.; Fernández-Díaz, L.; Prieto, M.; Putnis, A. *Chem. Geol.* **2006**, *225*, 322–335.
(32) Browning, F. H.; Fogler, H. S. *Langmuir* **1996**, *12*, 5231–5238.
(33) Uchtmann, V. A. *J. Phys. Chem.* **1972**, *76*, 1304–1310.
(34) Ikeda, T.; Boero, M.; Terakura, K. *J. Chem. Phys.* **2007**, *127*, 074503.
(35) Lighstone, F. C.; Schwegler, E.; Allesh, M.; Gygi, F.; Galli, G. *ChemPhysChem* **2005**, *6*, 1745–1749.
(36) Van Cappellen, P.; Charlet, L.; Stumm, W.; Wersin, P. *Geochim. Cosmochim. Acta* **1993**, *57*, 3505–3518.
(37) Pokrovsky, O. S.; Mielczarski, J. A.; Barres, O.; Schott, J. *Langmuir* **2000**, *16*, 2677–2688.
(38) Parkhurst, D. L. Appelo; C. A. J. *U. S. Geological Survey Water-Resources Investigation Report* 99-4259; U.S. Geological Survey: Reston, VA, 1999; 312 pp.
(39) Popov, K.; Rönkkömäki, H.; Lajunen, L. H. J. *Pure Appl. Chem.* **2001**, *73*, 1641–1677.
(40) Deluchat, V.; Bollinger, J.-C.; Serpaud, B.; Caullet, C. *Talanta* **1997**, *44*, 897–907.
(41) Schindler, P. M.; Stumm, W. In *Aquatic Surface Chemistry*; Stumm, W., Ed.; Wiley: New York, 1987; pp 83−110.
(42) Kowacz, M.; Putnis, A. *Geochim. Cosmochim. Acta* **2008**, *72*, 4476–4487.
(43) Ruiz-Agudo, E; Kowacz, M.; Putnis, C. V.; Putnis, A. *Geochim. Cosmochim. Acta* **2010**, *74*, 1256–1267.
(44) Helm, L.; Merbach, A. E. *Coord. Chem. Rev.* **1999**, *187*, 151–181.
(45) Pokrovsky, O. S.; Schott, J. *Environ. Sci. Technol.* **2002**, *36*, 426–432.
(46) Dove, P. M.; Czank, C. *Geochim. Cosmochim. Acta* **1995**, *59*, 1907–1915.
(47) Marcus, Y. *Pure Appl. Chem.* **1987**, *59*, 1093–1101.
(48) Putnis, A.; Junta-Rosso, J. L.; Hochella, M. F. *Geochim. Cosmochim. Acta* **1995**, *59*, 4623–4632.
(49) Putnis, C. V.; Kowacz, M.; Putnis, A. *App. Geochem.* **2008**, *23*, 2778–2788.
(50) Fenter, P.; Geissbuhler, P.; DiMasi, E.; Srajer, G.; Sorensen, L. B.; Sturchio, N. C. *Geochim. Cosmochim. Acta* **2000**, *64*, 1221–1228.
(51) de Leeuw, N. H.; Parker, S. C. *J. Phys. Chem. B* **1998**, *102*, 2914–2922.
(52) Kerisit, S.; Parker, S. C. *J. Phys. Chem. B* **2003**, *107*, 7676–7682.
(53) de Leeuw, N. H.; Purton, J. A.; Parker, S. C.; Watson, G. W.; Kresse, G. *Surf. Sci.* **2000**, *452*, 9–19.
(54) McCarthy, M. I.; Schenter, G. K.; Scamehorn, C. A.; Nicholas, J. B. *J. Phys. Chem.* **1996**, *100*, 16989–16995.
(55) Hass, K. C.; Schneider, W. F.; Curioni, A; Andreoni, W. *J. Phys. Chem. B* **2000**, *104*, 5527–5540.
(56) Ruiz-Agudo, E.; Putnis, C. V.; Jiménez-López, C.; Rodríguez-Navarro, C. *Geochim. Cosmochim. Acta* **2009**, *73*, 3201–3217.
(57) Duffy, D. M.; Harding, J. H. *Langmuir* **2004**, *20*, 7637–7642.
(58) Didymus, J. M.; Oliver, P.; Mann, S.; DeVries, A. L.; Hauschka, P. V.; Westbroek, P. *J. Chem. Soc. Faraday Trans.* **1993**, *89*, 2891–2900.
(59) Amjad, Z. *Tenside, Surfactants, Deterg.* **1997**, *34*, 102–107.
(60) Bishop, M.; Bott, S. G.; Barron, A. R. *Chem. Mater.* **2003**, *15*, 3074–3088.

(61) Putnis, A. *Rev. Mineral. Geochem.* **2009**, *70*, 87–124.
(62) Putnis, C. V.; Tsukamoto, K.; Nishimura, Y. *Am. Mineral.* **2005**, *92*, 19–26.
(63) Chernov, A. A. *Modern Crystallography III. Crystal Growth*; Springer-Verlag: Berlin, 1984.
(64) Pérez-Garrido, C.; Fernández-Díaz, L.; Pina, C. M.; Prieto, M. *Surf. Sci.* **2007**, *601*, 5499–5509.
(65) Astilleros, J. M.; Pina, C. M.; Fernández-Díaz, L.; Putnis, A. *Chem. Geol.* **2003**, *193*, 93–107.
(66) Pinto, A. J.; Jiménez, A.; Prieto, M. *Am. Mineral.* **2009**, *94*, 313–322.